Colloids and Surfaces A: Physicochem. Eng. Aspects 526 (2017) 76–81

Contents lists available at ScienceDirect

Colloids and Surfaces A: Physicochemical and Engineering Aspects

journal homepage: www.elsevier.com/locate/colsurfa

Monitoring the fate of small silver nanoparticles during artificial digestion

Claudia Kästner[a], Dajana Lichtenstein[b], Alfonso Lampen[b], Andreas F. Thünemann[a,*]

[a] BAM Federal Institute of Materials Research and Testing, Unter den Eichen 87, 12205 Berlin, Germany
[b] Federal Institute for Risk Assessment, Max-Dohrn-Straße 8-10, 10589 Berlin, Germany

HIGHLIGHTS

- SAXS is useful for determination of particle size distributions in digestion fluids.
- Silver nanoparticles without food components aggregate strongly during digestion.
- Sizes of silver nanoparticles are constant in saliva and stomach but particles were etched in the intestine.
- Milk powder is an excellent colloidal stabilizer and prevents aggregation and etching during digestion.

GRAPHICAL ABSTRACT

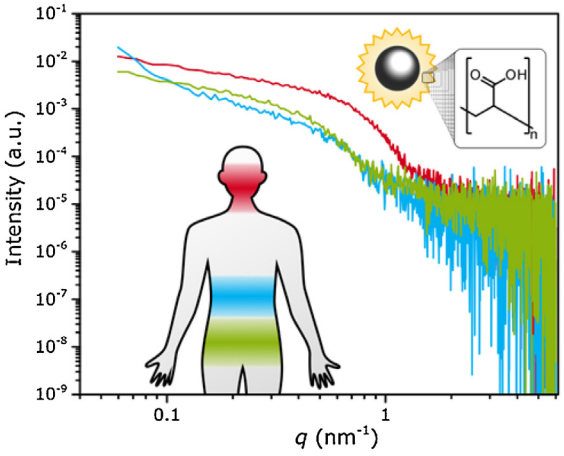

ARTICLE INFO

Article history:
Received 4 July 2016
Received in revised form 12 August 2016
Accepted 13 August 2016
Available online 16 August 2016

Keywords:
Artificial digestion
Food components
Small-angle X-ray scattering
SAXS

ABSTRACT

We report on the results of an *in vitro* digestion study of silver nanoparticles in presence and absence of food. The particles were poly(acrylic acid) stabilized ultra-small silver nanoparticles with a radius of 3.1 nm and a relative size distribution width of 0.2. As food components oil, starch, skimmed milk powder and a mixture thereof were chosen. Aggregation of the particles was quantified with small-angle X-ray scattering in terms of log-normal radii distributions. Complete aggregation of the primary particles was determined in the absence of food. In contrast, the presence of oil and starch initiates a disaggregation in the intestine. Only small aggregates of 6 nm radii and aggregation numbers of 7 were found in the presence of milk powder. It prevents primary particles from etching in the gastric and intestinal juice. Our results indicate that the silver nanoparticles can pass the digestion process in a nanoscale form but undergo a strong and food-dependent transformation in their state of aggregation.

1. Introduction

The use of silver nanoparticles in consumer related products has significantly increased over the last decade due to their special antimicrobial properties [1]. The estimated global production

* Corresponding author.
E-mail address: andreas.thuenemann@bam.de (A.F. Thünemann).

http://dx.doi.org/10.1016/j.colsurfa.2016.08.013

Table 1
Composition of the artificial digestion juices for saliva, stomach and intestine.

Compound	Supplier	Amount
Saliva		
NaCl	NeoLab	12.5 mg
NaSCN	Carl Roth	3.8 mg
$Na_2SO_4 \cdot 10H_2O$	AppliChem	13.7 mg
$NaHCO_3$	NeoLab	3.8 mg
KCl	NeoLab	11.3 mg
KH_2PO_4	AppliChem	15 mg
$CaCl_2 \cdot 2H_2O$	NeoLab	3.8 mg
Uric acid	AppliChem	2.5 mg
Urea	AppliChem	0.3 mg
Mucin	Sigma-Aldrich	18.8 mg
α-Amylase	Sigma-Aldrich	6.3 mg
Gastric juice		
NaCl	NeoLab	72.5 mg
KCl	NeoLab	17.5 mg
KH_2PO_4	AppliChem	6.7 mg
Mucin	Sigma-Aldrich	75 mg
Pepsin	AppliChem	25 mg
Intestinal juice		
NaCl	NeoLab	7.5 mg
$CaCl_2 \cdot 2H_2O$	NeoLab	12.5 mg
$MgCl_2 \cdot 6H_2O$	NeoLab	5 mg
$NaHCO_3$	NeoLab	25 mg
Bile extract porcine	Sigma-Aldrich	225 mg
Pancreatin	Sigma-Aldrich	225 mg
Trypsin	AppliChem	7.5 mg
Urea	AppliChem	7.5 mg

amounts to 55 tons per year [2]. Today silver nanoparticles are contained in a high variety of products from cosmetics like tooth pastes, to textiles, to children's toys and to dietary supplements [3]. The estimated humans' dietary intake of silver is 70–90 μg per day [5] which can be individually substantially higher due to the widespread application of silver nanoparticles. The unique properties of the nanoparticles are strongly depending on the surrounding conditions. Temperature, pH and salts can alter the particle characteristics by changing the size and size distribution through aggregation [6,7]. Additionally the surface chemistry and the interaction with biomolecules are crucial factors in determining the properties of nanoparticles [8]. For the different uptake mechanisms this is especially important for orally ingested particles. Thereby, the particles pass different digestion steps where physicochemical parameters like the pH are shifted over a wide range. The steps of an *in vivo* digestion contain the introduction of the nanoparticles in the saliva which is followed by the exposure to the gastric and intestinal juices. Hence, different mechanisms are possible, which include aggregation, enhanced ion release or *de novo* particle formation [9,10].

Most studies regarding the toxicological potential of silver nanoparticles are focused on their intestinal uptake and interaction with different cell types like M-cells or Caco-2-cells [11]. But considering different altering mechanisms during the digestion process the question arises whether the silver particles can pass the different digestion steps in a nanoscale form. These complex interactions between particles and the surrounding conditions can only be investigated in an *in vitro* model. Therefore, as previously reported [12], we used an artificial digestion procedure, which is based on the German standard DIN 19378 [13]. We adjusted this procedure in the present study for the digestion of silver nanoparticles (Fig. 1). It simulates the three steps of the gastro-intestinal passage by mimicking the oral, gastric and small intestinal conditions. These contain all relevant factors for a realistic environment such as pH changes, transit times between the different digestion steps, enzymes and digestive juices. Furthermore, the addition of food components completes the simulation of a realistic digestion process in a human body. Previous studies only considered the digestion without food components [10]. Detailed investigations regarding the influence of food components on changes of the size distribution of silver nanoparticles are still lacking [14].

We synthesized ultra-small silver nanoparticles with a core radius of 3 nm and poly(acrylic acid) as stabilizer for their application in the artificial digestion process. To evaluate possible changes in their characteristics, including core sizes, shapes and size distributions, we used small-angle X-ray scattering (SAXS). The advantages of this technique are (i.) an easy sample preparation, (ii.) a non-destructive measurement and (iii.) a statistically representative particle ensemble average. The silver particles can be measured directly in the saliva, in the gastric or the intestinal juice without purification or separation from the juices [10]. The measurement time amounts to 20 min. Additionally due to the use of X-rays with a wavelength of 0.154 nm the characterization of dispersed nanoparticles with radii from 1 nm to 60 nm is possible [15].

The aim of this study is to reveal the impact of digestion on the colloidal stability of very small silver nanoparticles for two different scenarios: Digestion with and without food additives. As representative food components we chose oil, starch, skimmed milk powder and a mixture of these three components in order to mimic realistic food surroundings.

2. Materials and methods

2.1. Materials

For the synthesis of nanoparticles silver nitrate was obtained from AppliChem, poly(acrylic acid) (M_w = 1800 g/mol) from Sigma Aldrich, ethylene glycol from Acros and sodium hydroxide from Fisher Scientific. Chemicals for the artificial digestion were purchased from Merck, Sigma-Aldrich, JT Baker or AppliChem in the highest available purity (Table 1). The food components are available supermarket products: Native olive oil from Pietro Coricelli Spa, Sucofin skimmed milk powder from Tsi GmbH & Co. KG and Mondamin starch (corn starch) from Unilever. Ultrapure water was used for all preparations (Milli-Q, 18.2 mΩ at 25 °C).

2.2. Preparation of nanoparticles

For the synthesis of silver nanoparticles silver nitrate and poly(acrylic acid) (M_w = 1800 g/mol) were used in a modified polyol process according to Hu et al. [16]. For the work-up phase the procedure was changed. Therefore no centrifugation was necessary and the particles were washed three times with excessive slight acidic water (pH 5). After washing the particles they settled over night and the supernatant was separated by decantation. The particles were dispersed in water and the pH was adjusted to a value of 11 with a solution of 5 wt% NaOH. The particles were characterized by SAXS and used in an artificial digestion process.

2.3. Artificial digestion

The *in vitro* digestion was applied as described previously by Lichtenstein et al. [12]. Firstly 1 mL of nanoparticle dispersion (3 g/L) was added to 7.5 mL artificial saliva with a pH of 6.4. The mixture was incubated under stirring for 5 min in a water bath at a temperature of 37 °C. After adding 17.5 mL of artificial gastric juice the pH was adjusted to a value of 2 with a solution of 10 wt% HCl and the suspension was incubated at 37 °C for 2 h. In the last step the addition of 25 mL of artificial intestinal juice was followed by adjusting the pH to 7.5 by adding $NaHCO_3$. The suspension was incubated under stirring at a temperature of 37 °C for 2 h. The ingredients of the artificial digestion juices are listed in Table 1. The *in vitro* digestion was additionally conducted in presence of the food

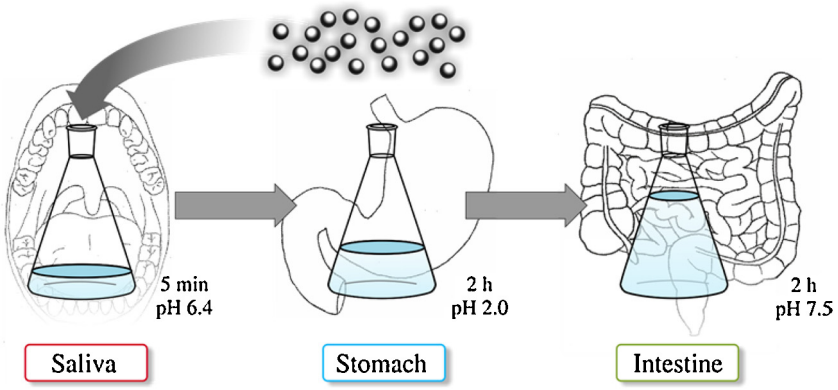

Fig. 1. Sketch of the artificial digestion of silver nanoparticles following three stages: saliva, gastric and intestinal tract. The path taken by the particles is indicated by arrows. Residence times and pH values are reported.

components starch, oil, skimmed milk powder (50 mg of each) and a mixture of those (50 mg of each resulting in 150 mg food).

2.4. Small-angle X-ray scattering (SAXS)

SAXS measurements were performed in a quartz-capillary with a Kratky-type instrument (SAXSess from Anton Paar, Austria) at 25 ± 1 °C. The SAXSess has a low sample-to-detector distance (0.309 m), which is appropriate for investigation of dispersions with low scattering intensities. The measured intensity was corrected by subtracting the intensity of a capillary filled with pure water. The scattering vector is defined in terms of the scattering angle q and the wavelength λ of the radiation ($\lambda = 0.154$ nm): thus $q = 4\pi n \lambda^{-1} \sin\theta$. Deconvolution (slit length desmearing) of the SAXS curves was performed with the SAXS-Quant software. Curve simulations were performed using a Monte-Carlo Method with the software McSAS [17]. The resulting cumulative distribution functions were fitted with Eq. (1) to reveal the parameters summarized in Figs. 4–6.

The error bars in Figs. 4–6 represent the standard errors as determined from the least-squares optimization method implemented in the Origin 10 software. In principle, these uncertainties can be utilized to determine the combined standard uncertainties from all SAXS input quantities. For more information we refer to a study of the traceability of determination of the size distribution of nanoparticles by Meli et al. [18]. However, this is a tedious procedure which is beyond the scope of this work. We have been shown earlier in a work on the SASfit data evaluation program that the uncertainties of the size parameters from the fitting procedure are of the same order of magnitude as the combined standard uncertainties.

3. Results and discussion

3.1. Digestion in absence of food components

The artificial digestion according to a standardized procedure [13] is structured in three stages: Saliva, stomach and intestine. The digestion juices containing the particles were measured with SAXS for 20 min directly after incubation. Volume-weighted radii distributions were determined from the SAXS data using a Monte Carlo SAXS data analysis [19]. This new type of data evaluation is form-free, which means that no *a priori* choice of the type of size distribution is needed as normally necessary [20]. We found radii distributions which can be interpreted as result of mixtures of primary particles and aggregates. We found that the following sum of

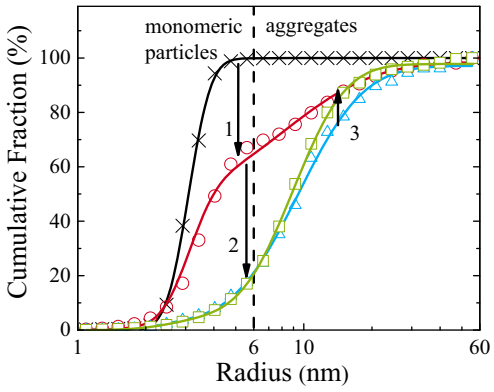

Fig. 2. Volume-weighted radii distribution of silver nanoparticles derived by SAXS measurements. Shown are pristine particles and particles after the three stages of artificial digestion: Saliva, stomach and intestine (black crosses, red spheres, blue triangles and green squares, respectively) in cumulative fraction presentation. Particles were digested without food components. The solid lines are best fit curves according to Eq. (1). The path of digestion is indicated by numbered arrows. (For interpretation of the references to color in this figure legend, the reader is referred to the web version of this article.)

two cumulative lognormal distribution functions is useful for the quantification of the distributions for all stages of digestion:

$$F(R) = \frac{a_1}{2}\operatorname{erfc}\left(\frac{\log\left(\frac{R_{0,1}}{R}\right)}{\sqrt{2}w_1}\right) + \frac{a_2}{2}\operatorname{erfc}\left(\frac{\log\left(\frac{R_{0,2}}{R}\right)}{\sqrt{2}w_2}\right). \quad (1)$$

Therein the a_i are scaling factors, which are a measure for the volume fraction of primary particles and aggregates, respectively. The w_i are width parameters and the $R_{0,i}$ are the median radii. Using these parameters, the mean radii were calculated as $R_i = R_{0,i} e^{w_i^2/2}$ and the relative standard $\sigma_i/R_i = \sqrt{e^{2\sigma^2} - e^{\sigma^2}}$ deviations of the width of the size distributions as

First, we found that the radii distribution of the pristine particles display a mean radius of $R_1 = (3.1 \pm 0.1)$ nm and a relative distribution width of $\sigma_1 = 0.2$. The second term in Eq. (1) was zero, which means, that no indication for the presence of aggregates was found. An amount of 100% of particles is smaller than 6 nm as can be seen in Fig. 2(a) (black crosses are data points and the black solid curve correspond to the best fit applying Eq. (1)). Note that only the silver core of the particles can be "seen" with SAXS while the stabilizing shell of poly(acrylic acid) is practically invisible due to the large X-ray scattering contrast of silver. The particles are stable at a basic pH, but aggregate at acidic pH. Therefore, as expected, aggregation took place when the primary particles were incubated in the saliva

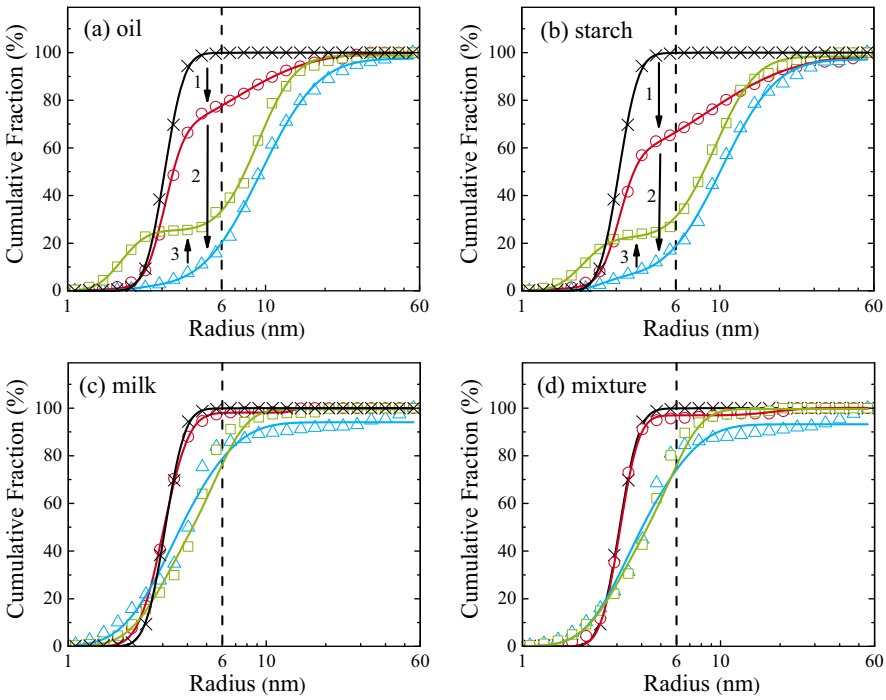

Fig. 3. Volume-weighted radii distributions of silver nanoparticles of pristine particles (black crosses) and at the three stages of artificial digestion: Saliva, stomach and intestine (red circles, blue triangles and green squares, respectively) in cumulative fraction presentation. Particles were digested with oil (a), starch (b), skimmed milk powder (c) and a mixture of all components (d). The solid lines are best fit curves utilizing Eq. (1). The dashed vertical line at a radius of 6 nm indicates the upper limit of the radius of primary particles. (For interpretation of the references to color in this figure legend, the reader is referred to the web version of this article.)

at pH 6.4 for 5 min (indicated by arrow 1 directed towards red circles in Fig. 2). Only 48 % of the primary particles are present. The rest forms aggregates with a mean radius of $R_2 = (8 \pm 2)$ nm and a relative width of $\sigma_2 = 0.31$. We estimated the aggregation number from the ratio of the volume of an aggregate to the volume of a primary particle as $N_{agg} = R_2^3/R_1^3$. From this follows that the aggregates consist of about (21 ± 13) primary particles.

The second step of digestion includes the incubation at pH 2 in the stomach for 2 h (indicated by arrow 2 towards blue triangles in Fig. 2). After this stage the size of the primary particles decreased to $R_1 = (2.2 \pm 0.7)$ nm and their relative fraction decreased to (3 ± 2) %. The remaining particles form aggregates with a mean radius of $R_2 = (9 \pm 1)$ nm and a relative width of $\sigma_2 = 0.23$. Due to the small fraction of primary particles a reliable determination of the aggregation number is not possible. The final step is the incubation in the intestinal juice at pH 7.5 for 2 h (indicated by arrow 3 towards green squares in Fig. 2). Now the radius of the primary particles amounts to $R_1 = (2.6 \pm 0.7)$ nm and the volume fraction of primary particles stays constant. The aggregates display a mean radius of $R_2 = (9 \pm 1)$ nm with a relative width of $\sigma_2 = 0.18$.

As a first summary we can conclude that the radii of the primary particles decrease in the stomach in the course of digestion (see Fig. 4). Most of the particles form immediately aggregates in the saliva. Only a few primary particles are present in the stomach and intestine (see Fig. 5). Fit data are summarized in Table 2.

With dynamic light scattering it is typically possible to "see" the whole particle, *i.e.* core plus its shell. Therefore, a combination of SAXS and DLS data allows often to estimate the thickness of the particles' shell [21]. The problem to apply this procedure for our system is that the particles are directly measured in the turbid digestion fluids. Unfortunately, DLS provides no meaningful results for particles in such turbid media.

Table 2
Characteristics of primary particles and aggregates in pristine state and after the digestion stages saliva, stomach and intestine resultant from curve fits applying Eq. (1). Given are the primary particles radii (R_1), their relative volume fraction (Fraction), the radii of the aggregates (R_2), their relative distribution width (σ_2) and average aggregation numbers of primary particles per aggregate (N_{agg}). The relative width of σ_1 is in the range of 0.1–0.2 and the uncertainty of R_1 is ±0.1 nm.

Food	R_1 (nm)	Fraction (%)	R_2 (nm)	σ_2	N_{agg}
Pristine silver particles					
	3.1	100	–[a]	–[a]	–[a]
Particles in saliva					
None	3.1	48 ± 10	8 ± 2	0.31	21 ± 13
Oil	3.1	62 ± 3	7 ± 1	0.30	13 ± 3
Starch	3.1	51 ± 2	9 ± 1	0.35	25 ± 4
Milk	3.1	100	–[a]	–[a]	–[a]
All	3.1	100	–[a]	–[a]	–[a]
Particles in stomach					
None	2.2	3 ± 2	9 ± 1	0.23	80 ± 2
Oil	2.2	2 ± 2	9 ± 1	0.23	86 ± 2
Starch	2.5	6 ± 2	10 ± 1	0.22	66 ± 2
Milk	3.1	72 ± 14	6 ± 2	0.16	7 ± 9
Mixture	3.1	60 ± 15	6 ± 2	0.16	7 ± 6
Particles in intestine					
None	2.6	5 ± 2	9 ± 1	0.18	42 ± 2
Oil	1.9	25 ± 1	9 ± 1	0.15	117 ± 4
Starch	2.0	22 ± 1	9 ± 1	0.16	103 ± 5
Milk	3.1	57 ± 6	6 ± 1	0.16	7 ± 2
Mixture	3.1	56 ± 5	6 ± 1	0.11	7 ± 1

[a] No aggregates were detected.

3.2. Digestion in the presence of food

The digestion of the particles was repeated in the presence of oil, starch, milk and a mixture thereof. The resulting distributions of the radii and curve fits utilizing Eq. (1) are shown in Fig. 3 (a)–(d).

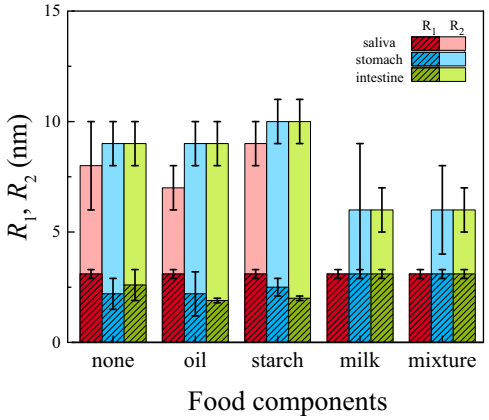

Fig. 4. Mean radii of the primary silver nanoparticles, R_1, and radii of their aggregates, R_2, as a function of different food components. The radii are presented according to the three stages of the digestion process: Saliva, stomach and intestine (red, blue and green bars, respectively). (For interpretation of the references to color in this figure legend, the reader is referred to the web version of this article.)

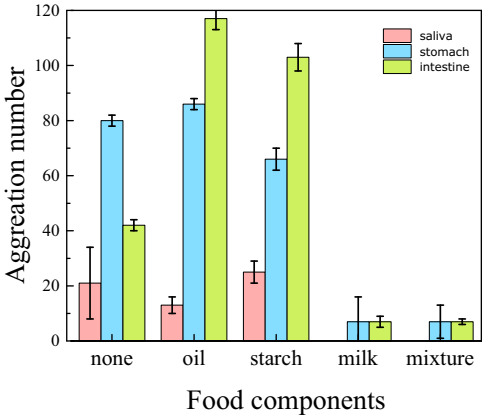

Fig. 6. Aggregation numbers of silver nanoparticles as a function of different food components. The presented fractions are assigned to saliva, stomach and intestine (red, blue and green bars, respectively). (For interpretation of the references to color in this figure legend, the reader is referred to the web version of this article.)

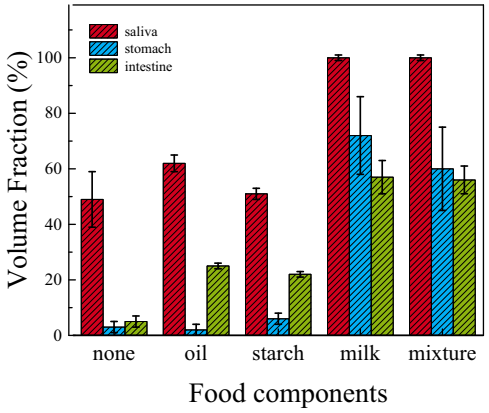

Fig. 5. Volume fractions of primary silver nanoparticles as a function of different food components. The presented fractions are assigned to saliva, stomach and intestine (red, blue and green bars, respectively). (For interpretation of the references to color in this figure legend, the reader is referred to the web version of this article.)

Fit parameters are summarized in Table 2. From the inspection of the figures and the fit parameters it is obvious that the presence of food strongly influences the aggregation behavior compared to the situation without food. Furthermore, curves and parameters in the presence of oil and starch are similar. Also the curves and the parameters for the presence of milk and food mixture are similar.

When looking first at the primary particle radii we note that they are constant in saliva in all cases like they were in the absence of food. Then the radii decrease in the stomach from 3.1 nm to 2.5 nm and 2.2 nm in the presence of oil and starch, whereas no reduction was observed for milk and food mixture.

Additionally, the size of the aggregates is nearly the same in the presence of food and without. In saliva the aggregates' radii are (7 ± 1) nm for oil and (9 ± 1) nm for starch while no aggregates were found for milk and food mixture. The aggregates' radii in stomach and intestine are very similar for oil (9 ± 1) nm and starch (10 ± 1) nm and only very small aggregates of 6 nm radius were detectable for milk and food mixture (see Fig. 3). Interestingly, the volume fraction of primary particles displays a deep minimum of ca. 2% and 6% in the stomach followed by an increase to 25% and 22% in the intestine for oil and starch, respectively. In contrast, fraction of ca. 100% primary particles were found in saliva for milk and food mixture. This is followed by a continuous decrease to 72% for milk and 60 % for mixture in the stomach. Final values were 57% for milk and 56% for food mixture in the intestine. The aggregation numbers in presence of oil increase successively in the line $N_{agg} = (13 \pm 3)$, (86 ± 2) and (117 ± 4) and similarly in the presence of starch in the line $N_{agg} = (25 \pm 4)$, (66 ± 2) and (103 ± 5). In contrast, small aggregation numbers of about 7 were found for milk and food mixture in stomach and intestine (Fig. 6).

Our findings show, that all food components have a strong colloidal stabilizing effect in comparison to the situation without additives. Oil and starch are similar in their stabilization properties and the size of aggregates is limited to radii of ca. 10 nm and maximum aggregation numbers of ca. 100. Milk and food mixture are the strongest in preventing particle's aggregation. Here the size of aggregates is limited to radii of ca. 6 nm with aggregation numbers of ca. 7. Moreover, only in the presence of milk proteins no radii reduction of the primary particles was observed after intestinal incubation. We attribute these findings to the strong colloidal stabilizing properties of milk proteins. The surprising increase of the fraction of primary particles from stomach to intestine in the presence of oil may be explained by the presence of lipase in the latter. The artificial intestinal juice is composed of pancreatin which mainly contains lipase. This enzyme catalyzes the hydrolysis of fats just like the used oil. Therefore, we assume that the oil is converted to fatty acids, which stabilize the primary particles and lead to their increase. Similarly, we assume that stabilizing oligosaccharides were formed by the hydrolysis of starch due to the enzyme amylase, which is present in the pancreatin. That could explain the increase of primary particles from stomach to intestine in the presence of starch.

4. Conclusion

During artificial digestion of silver nanoparticles with radii of 3 nm, the size and size distribution remain in a nanoscale but undergo a transformation in the ratio of primary particles and aggregates. It was observed that skimmed milk powder shows a stabilizing and protecting effect for the application and interaction with food components. In this case the size distribution did not change significantly, whereas the addition of oil and starch produced a transformation in the radii distribution and a partial disaggregation. Therefore, the addition of food components can strongly effect changes in the size distribution of silver nanoparticles during the digestion process.

References

[1] R. Foldbjerg, X. Jiang, T. Miclaus, C. Chen, H. Autrup, C. Beer, Silver nanoparticles – wolves in sheep's clothing? Toxicol. Res. 4 (2015) 563–575.
[2] F. Piccinno, F. Gottschalk, S. Seeger, B. Nowack, Industrial production quantities and uses of ten engineered nanomaterials in Europe and the world, J. Nanopart. Res. 14 (2012) 1–11.
[3] K.R. Rogers, K. Bradham, T. Tolaymat, D.J. Thomas, T. Hartmann, L. Ma, A. Williams, Alterations in physical state of silver nanoparticles exposed to synthetic human stomach fluid, Sci. Total Environ. 420 (2012) 334–339.
[5] S.W.P. Wijnhoven, W.J.G.M. Peijnenburg, C.A. Herberts, W.I. Hagens, A.G. Oomen, E.H.W. Heugens, B. Roszek, J. Bisschops, I. Gosens, D. Van De Meent, S. Dekkers, W.H. De Jong, M. van Zijverden, A.J.A.M. Sips, R.E. Geertsma, Nano-silver – a review of available data and knowledge gaps in human and environmental risk assessment, Nanotoxicology 3 (2009) 109–138.
[6] A. Bruinink, J. Wang, P. Wick, Effect of particle agglomeration in nanotoxicology, Arch. Toxicol. 89 (2015) 659–675.
[7] A. Nel, T. Xia, L. Mädler, N. Li, Toxic potential of materials at the nanolevel, Science 311 (2006) 622–627.
[8] L. Rizzello, P.P. Pompa, Nanosilver-based antibacterial drugs and devices: mechanisms, methodological drawbacks, and guidelines, Chem. Soc. Rev. 43 (2014) 1501–1518.
[9] J. Liu, R.H. Hurt, Ion release kinetics and particle persistence in aqueous nano-silver colloids, Environ. Sci. Technol. 44 (2010) 2169–2175.
[10] L. Böhmert, M. Girod, U. Hansen, R. Maul, P. Knappe, B. Niemann, S.M. Weidner, A.F. Thünemann, A. Lampen, Analytically monitored digestion of silver nanoparticles and their toxicity on human intestinal cells, Nanotoxicology 8 (2014) 631–642.
[11] H. Bouwmeester, J. Poortman, R.J. Peters, E. Wijma, E. Kramer, S. Makama, K. Puspitaninganindita, H.J.P. Marvin, A.A.C.M. Peijnenburg, P.J.M. Hendriksen, Characterization of translocation of silver nanoparticles and effects on whole-genome gene expression using an in vitro intestinal epithelium coculture model, ACS Nano 5 (2011) 4091–4103.
[12] D. Lichtenstein, J. Ebmeyer, P. Knappe, S. Juling, L. Böhmert, S. Selve, B. Niemann, A. Braeuning, A.F. Thünemann, A. Lampen, Impact of food components during in vitro digestion of silver nanoparticles on cellular uptake and cytotoxicity in intestinal cells, Biol. Chem. 396 (2015) 1255–1264.
[13] D. 19738, Bodenbeschaffenheit – Resorptionsverfügbarkeit von organischen und anorganischen Schadstoffen aus kontaminiertem Bodenmaterial, 2004–07.
[14] S. Gaillet, J.-M. Rouanet, Silver nanoparticles: their potential toxic effects after oral exposure and underlying mechanisms – a review, Food Chem. Toxicol. 77 (2015) 58–63.
[15] O. Glatter, O. Kratky, Small Angle X-Ray Scattering, Academic Press, London, 1982.
[16] Y. Hu, J. Ge, D. Lim, T. Zhang, Y. Yin, Size-controlled synthesis of highly water-soluble silver nanocrystals, J. Solid State Chem. 181 (2008) 1524–1529.
[17] B.R. Pauw, Everything SAXS: small-angle scattering pattern collection and correction, J. Phys.-Condens. Matter 25 (2013) 383201.
[18] F. Meli, T. Klein, E. Buhr, C.G. Frase, G. Gleber, M. Krumrey, A. Duta, S. Duta, V. Korpelainen, R. Bellotti, G.B. Picotto, R.D. Boyd, A. Cuenat, Traceable size determination of nanoparticles, a comparison among European metrology institutes, Meas. Sci. Technol. 23 (2012) 125005.
[19] I. Bressler, B.R. Pauw, A.F. Thunemann, McSAS: software for the retrieval of model parameter distributions from scattering patterns, J. Appl. Crystallogr. 48 (2015) 962–969.
[20] I. Bressler, J. Kohlbrecher, A.F. Thunemann, SASfit: a tool for small-angle scattering data analysis using a library of analytical expressions, J. Appl. Crystallogr. 48 (2015) 1587–1598.
[21] A.F. Thunemann, S. Rolf, P. Knappe, S. Weidner, In situ analysis of a bimodal size distribution of superparamagnetic nanoparticles, Anal. Chem. 81 (2009) 296–301.